Journal of Archaeological Science 36 (2009) 1516–1526

Contents lists available at ScienceDirect

Journal of Archaeological Science

journal homepage: http://www.elsevier.com/locate/jas

Magnetic detection of ship ballast deposits and anchorage sites in King Herod's Roman harbour, Caesarea Maritima, Israel

Joseph I. Boyce [a,*], Eduard G. Reinhardt [a], Beverly N. Goodman [b]

[a] School of Geography and Earth Sciences, McMaster University, 1280 Main St. West, Hamilton, Ontario, Canada L8S 4K1
[b] Interuniversity Institute for Marine Sciences, Eilat 88103, Israel

ARTICLE INFO

Article history:
Received 14 October 2008
Received in revised form
25 February 2009
Accepted 2 March 2009

Keywords:
Caesarea Maritima
Harbour
Ballast
Anchorages
Magnetic survey

ABSTRACT

Ballast stone deposits are a common feature of sediments in ancient harbour basins but are often overlooked as a potential source of archaeological information. Recent geophysical investigations at Caesarea Maritima in Israel have discovered a thick, laterally extensive ballast layer in the area seaward of the 1st c. BC Roman harbour. The ballast deposits were identified by low-relief mounds on the seabed with elevated magnetic intensities. Jet probing and excavation of magnetic anomalies at several locations revealed a 20–60 cm thick rubble layer containing large quantities of Late Roman and Byzantine pottery, local sedimentary boulders (kurkar sandstone, limestone cobbles) and foreign igneous and metamorphic boulders (granite, schist, volcanics; ca. 50%). The foreign boulders and pottery identify the rubble layer as ballast and ships refuse jettisoned by merchant ships outside the harbour. The strong magnetic contrast between the ballast deposits and the natural seabed sediments is attributed to the high magnetic susceptibility ($>10^{-3}$ SI) of crystalline boulders and pottery materials within the ballast rubble.
AMS ^{14}C and OSL dates and pottery evidence indicate the ballast accumulation began in the Late Roman period (ca. 200–330 AD) and continued well into the Late Byzantine (ca. 7th c. AD). The main phase of ballast deposition (ca. 4th–5th c. AD) coincided with a decline in the state of Caesarea's harbour following a destructive tsunami event in the early 2nd c. AD and records a shift to a more intensive use of the area seaward of the harbour as an anchorage and ballast lightening area.

1. Introduction

Ballast stone deposits are a common feature of bottom sediments in ancient harbours and anchorage sites where merchant ships jettisoned ballast prior to lading of cargo (Raveh and Kingsley, 1991; McManus, 1999; Stanley and Bernasconi, 2004; Reinhardt et al., 2006). Typically these deposits consist of a heterogeneous mixture of ballast stones admixed with locally derived sediments and varying quantities of pottery and other ship refuse. In harbours with a long history of maritime trade, the jettisoning of ballast stones over several centuries can result in formation of a thick, laterally extensive deposit (e.g. Reinhardt and Raban, 1999). Ballast deposits also occur as discrete stone piles and mounds on the seabed, marking the location of shipwreck sites (Parker, 1981; Keith and Simmons, 1985; Ballard et al., 2000; Callahan et al., 2001; Bertrame and Gaddi, 2002; Raveh and Kingsley, 1992; Kingsley, 2003; Royal, 2006). These are formed when wooden hull structures are destroyed during wrecking or lost to decay and erosion processes, and where preserved, can provide a record of the hull contents. The petrologic and geochemical analysis of shipwreck ballast materials (so-called 'ballastology') can also provide important clues for determining shipwreck identity (Lamb, 1986). Conaghan et al. (1998) for example identified the origin of a 19th-century shipwreck in northern Queensland based on ballast petrographic characteristics and Lamb et al. (1990) used a similar approach to identify ports visited by a 16th-century wreck in the West Indies. Other workers have employed ballast characteristics to infer historical shipping trade routes (McManus, 1999; Lazareth et al., 2001) and to estimate hull size and wrecking conditions (Keith and Simmons, 1985).

The application of petrographic and geochemical analysis to ballast in ancient harbour sediments is likely to be more problematic. In ports with a long history of sea-faring trade ballast composition is likely to be very heterogeneous, reflecting many different geographic locations and geological sources; accordingly, ballast provenience is often complex and difficult to interpret in terms of shipping trade routes or cargo origin (Keith and Simmons, 1985; Raban, 2004). Votruba (2007) for example examined imported cobble and ballast stones used in the construction of Caesarea's Roman harbour and was able to identify local versus

* Corresponding author. Tel.: +1 905 525 9140x24188; fax: +1 905 546 0463.
E-mail address: boycej@mcmaster.ca (J.I. Boyce).

0305-4403/$ – see front matter © 2009 Elsevier Ltd. All rights reserved.
doi:10.1016/j.jas.2009.03.007

foreign, far-travelled materials but not their specific source localities. Identification of source areas requires that the ballast materials have a distinctive lithologic or geochemical 'fingerprint' that can be linked to a specific geographic location (e.g. Emery et al., 1968; Lazareth et al., 2001).

A more straightforward, but largely overlooked significance of ballast deposits, is that they can be used as an indicator of the relative intensity of past shipping activity and to identify the location of anchorage areas. McManus (1999) for example used petrographic evidence to identify ballast materials deposited by 19th century merchant vessels in the Tayport estuary in Scotland. He estimated that more than 100,000 tonnes of ballast had been accumulated over a 100-year period as a result of intensive historical shipping activities. Thick ballast stone layers have also been documented from a number of ancient harbour sites in the Mediterranean (e.g. Caesarea Maritima, Alexandria, Dor) (Reinhardt and Raban, 1999; Kingsley, 2003; Stanley and Bernasconi, 2004; Reinhardt et al., 2006) but have largely been disregarded as a potential archive of archaeological information, as there is a general perception that ballast layers are essentially *ex-situ* deposits, lacking proper stratigraphic and archaeological contexts (Parker, 1981; Lamb, 1986). Ballast deposits and associated pottery materials, however, can be preserved as *in-situ* layers under favorable environmental conditions; for example in low energy environments, such as sheltered harbour basins and in natural embayments where waves and currents are insufficient to erode or rework coarse deposits. Ballast layers can also be preserved on open, unprotected marine shelves when deposited below the storm wave base, and in shallow water (i.e. above storm wave base) when buried rapidly by subsequent storm deposition, as was the case at Caesarea (Reinhardt et al., 2006).

In this paper, we report on extensive *in-situ* ballast stone deposits discovered during a geophysical survey of King Herod's Roman harbour at Caesarea Maritima, in Israel (Fig. 1). The geophysical survey was conducted initially with the objective of mapping the submerged harbour architecture (Boyce et al., 2004) but also revealed several anomalous magnetic and bathymetric features in the area seaward of the Roman harbour (Fig. 1). These were investigated by jet probing and underwater excavations and identified as an extensive ballast rubble layer. The thickness and wide extent of the ballast layer at Caesarea indicates a sustained use of the area seaward of the Roman harbour after the 2–3rd c. AD (Late Roman Period) as a vessel anchorage and ballast unloading area. These findings corroborate other work that has documented the partial destruction of the harbour basin and its decline as a safe anchorage as a result of a 2nd c. AD tsunami event (Reinhardt et al., 2006). Thick ballast accumulations are a feature of many other ancient harbours and the methods and results reported here have broader application to other sites in the Mediterranean and elsewhere. The high magnetic susceptibility of the ballast materials at Caesarea also suggests the potential for magnetic detection of buried shipwreck ballast mounds in sandy shelf environments.

2. Study area and geoarchaeologic setting

The Roman port city of Caesarea Maritima is located on the northwest coast of Israel, about 40 km south of Haifa (Fig. 1). The city and its harbour were constructed under the rule of King Herod during the late 1st c. BC (Raban, 1992; Hohlfelder, 1999; Reinhardt and Raban, 1999; Raban et al., 1999). The ruined remains of the Roman harbour cover an area of about 10 ha and lie in water depths between 4 and 10 m. The harbour originally had three separate basins enclosed by a protective arched mole to the west and a narrow rectangular mole in the north (Fig. 1). The moles are now submerged more than 5 m below sea level and covered by a thick layer of collapsed rubble. The various phases in the construction of the harbour, its operation and subsequent destruction have been described in detail by Raban (1994) and others (Brandon, 1999; Hohlfelder, 1999; Reinhardt et al., 2006; Reinhardt and Raban, 2008).

In this study we describe an extensive ballast layer discovered in the shallow (ca. <10 m) inshore area to the west (seaward) of the Roman harbour ruins (Fig. 1). The inshore has a low relief, gently sloping bottom (Figs. 1, 3B) and consists predominantly of fine- to medium-grained sand and fine gravel with local surface concentrations of pottery sherds and other cultural debris (Reinhardt et al., 2006; Reinhardt and Raban, 2008). The shoreface sands are up to several metres in thickness and overlie Pleistocene-age eolianite sandstone bedrock known locally as 'kurkar' (Avnimelech, 1962; Gvirtzman et al., 1983).

3. Methods

3.1. Geophysical surveys

Geophysical investigations were conducted over a 1-km^2 area of the harbour and the inshore area at Caesarea (Fig. 2A). More than 100 line km of high-resolution magnetic and bathymetry data were acquired using a Marine Magnetics Seaspy™ (Overhauser) marine magnetometer and Garmin™ 200 kHz echosounder. The Overhauser sensor has the advantages of high sensitivity (0.01 nT/$\sqrt{}$Hz) and does not suffer from heading errors that limit the use of optically pumped alkali vapour magnetometers. The magnetometer was towed behind an inflatable boat at a speed of 2–4 knots at a depth of 1–2 m below the water surface. The sensor altitude was also recorded with each magnetic measurement to allow for later correction of the water depth-related changes in magnetic intensity. The magnetometer sample rate was 0.25 s (4 Hz) yielding an inline measurement interval of ca. 0.25–1 m. The survey lines were oriented in north–south and west–east directions with nominal line spacing of 10–20 m (Fig. 2A). A second base-station magnetometer was deployed onshore for the duration of the survey to continuously record the diurnal magnetic variation. Survey positioning was provided by an onboard D-GPS (sub-metre Trimble RTK 4600) receiving differential correction data from an onshore base receiver.

The post-survey processing of magnetic data included diurnal and lag corrections, tie-line levelling and drape corrections (Luyendyk, 1997; Boyce et al., 2004). Drape corrections compensate for variations in the magnetic signal intensity produced by changes in the sensor altitude and seabed topography (Grauch and Campbell, 1984; Pilkington and Thurston, 2001). These corrections are routinely applied to aeromagnetic survey data to eliminate terrain effects (Ugalde and Morris, 2008), but are also applicable to marine surveys where the changes in water depth can generate significant changes in measured magnetic field (Pozza et al., 2004). As water depth increases for example, the magnetic signal intensity falls off with the inverse of the distance cubed for a typical dipole target (Breiner, 1973; Telford et al., 1998). Drape corrections were implemented in this study using the chessboard technique of Cordell (1985). The method uses upward and downward continuation of the magnetic signal to place all measurements at a constant height above the seabed, eliminating depth-related changes in signal intensity. The bathymetry data were corrected for sea-surface variations (waves, tides) using the D-GPS elevation data and tie-line leveled and gridded to produce a digital bathymetric elevation model following the procedures outlined by Sonnenburg and Boyce (2008).

To aid in interpretation of magnetic survey data, magnetic susceptibility measurements were obtained on representative samples of bottom sediments and a range of ballast stone types

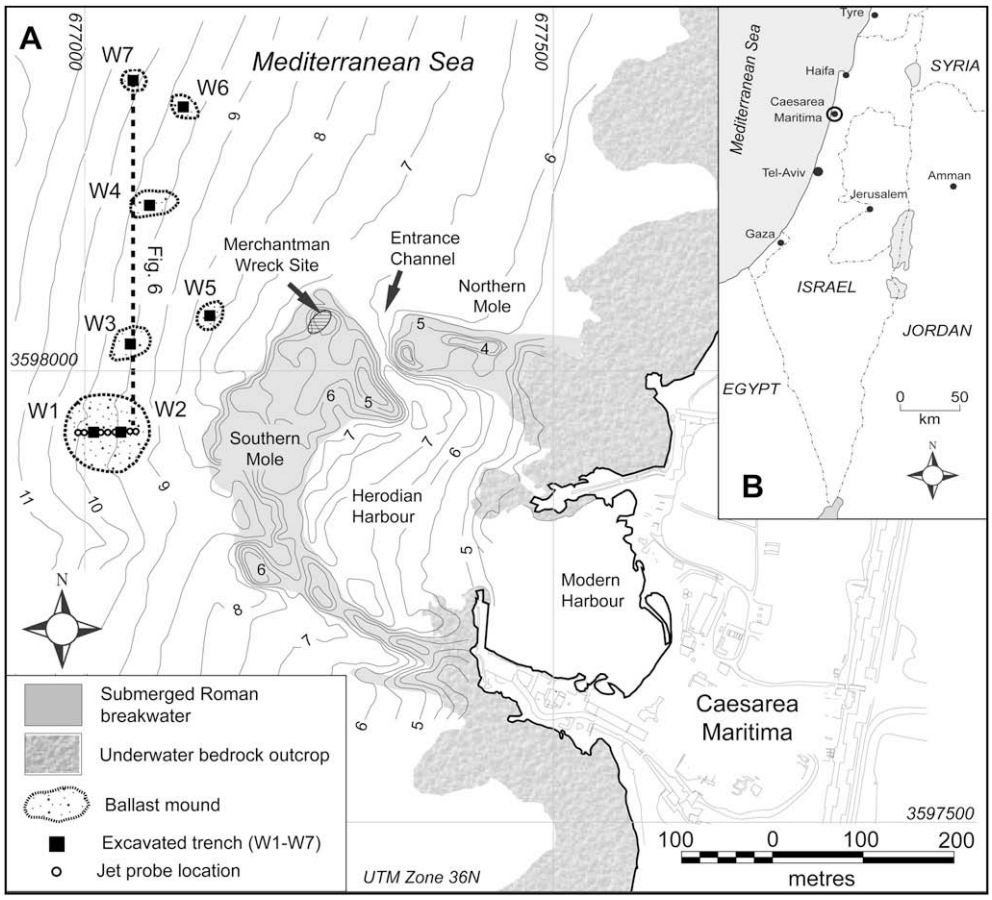

Fig. 1. A. Study area map showing submerged Roman harbour ruins, ballast mounds and locations of excavated trenches and sediment probes. Generalized bathymetric contours also shown (contour interval = 1 m). B. Location of study area in eastern Mediterranean.

retrieved from excavation trenches (Table 1). Volume magnetic susceptibility measurements (κ) were obtained on whole ballast stone samples using a Bartington (MS2-E1) surface measurement probe. A number of repeat surface measurements were made for each boulder sample and the average κ value taken. For sediment samples, volume susceptibility measurements were performed on 8–10 g dry sediment samples using a Bartington MS2-B susceptibility meter. Air measurements were performed before and after all susceptibility measurements in order to monitor and correct for instrument drift.

3.2. Trenches and sediment probes

Trenches were excavated at 7 sites to investigate the origin of the magnetic anomalies (Fig. 1A). Trenches 2–4 m in width were excavated to a depth of 1–3 m using a diver-operated water dredge (Reinhardt, 1999). At each site a detailed stratigraphic log was recorded and bulk sediment samples and ballast stones were collected for laboratory magnetic property analysis. At sites W6 and W7 shell materials were collected for dating using AMS ^{14}C methods and several sand samples for dating using OSL methods (Reinhardt et al., 2006; Rink and Reinhardt, 2008).

A series of sediment probes were conducted along a 100 m west–east transect (W1–W2; Fig. 1A) to the west of the harbour. The probes were carried out using a diver-operated water jet that was driven up to 3 m into the bottom sediment. The sediment probes provided a means of establishing the lateral continuity of the rubble layer between the excavated trenches and the thickness of the overlying sediment.

4. Results

4.1. Magnetic and bathymetry data

Magnetic and bathymetric maps of the inshore area at Caesarea are shown as colour-shaded images in Figs. 2B, 3 The magnetic map (Fig. 2B) shows variations in the Earth's total field intensity (in nanoteslas) produced by changes in the concentration of magnetic minerals (principally magnetite and titano-magnetites) within the seafloor sediments and bedrock. The large variations in magnetic intensity across the Roman harbour (Figs. 3, 4) result from the presence of magnetite-rich hydraulic concrete (pozzolana) within the buried harbour foundation (Brandon, 1999). The geophysical results for the Roman harbour have been discussed in detail elsewhere (Boyce et al., 2004) and we focus here on the area seaward of the harbour.

As shown in the bathymetry data (Fig. 3B), the area beyond the harbour is characterized by a gently sloping, low-relief shoreface that extends from the western edge of Herod's harbour into water depths of >10 m. The magnetic map (Fig. 3A) shows a relatively high magnetic relief across the harbour and adjacent areas with a total field variation of about 40 nT. An area of high magnetic intensity in the northeast corner of the map (Fig. 3A) corresponds with iron-rich sandstone bedrock and *hamra* (terra rosa soil) that forms the modern shoreline at Caesarea (Avnimelech, 1962; Boyce et al., 2004).

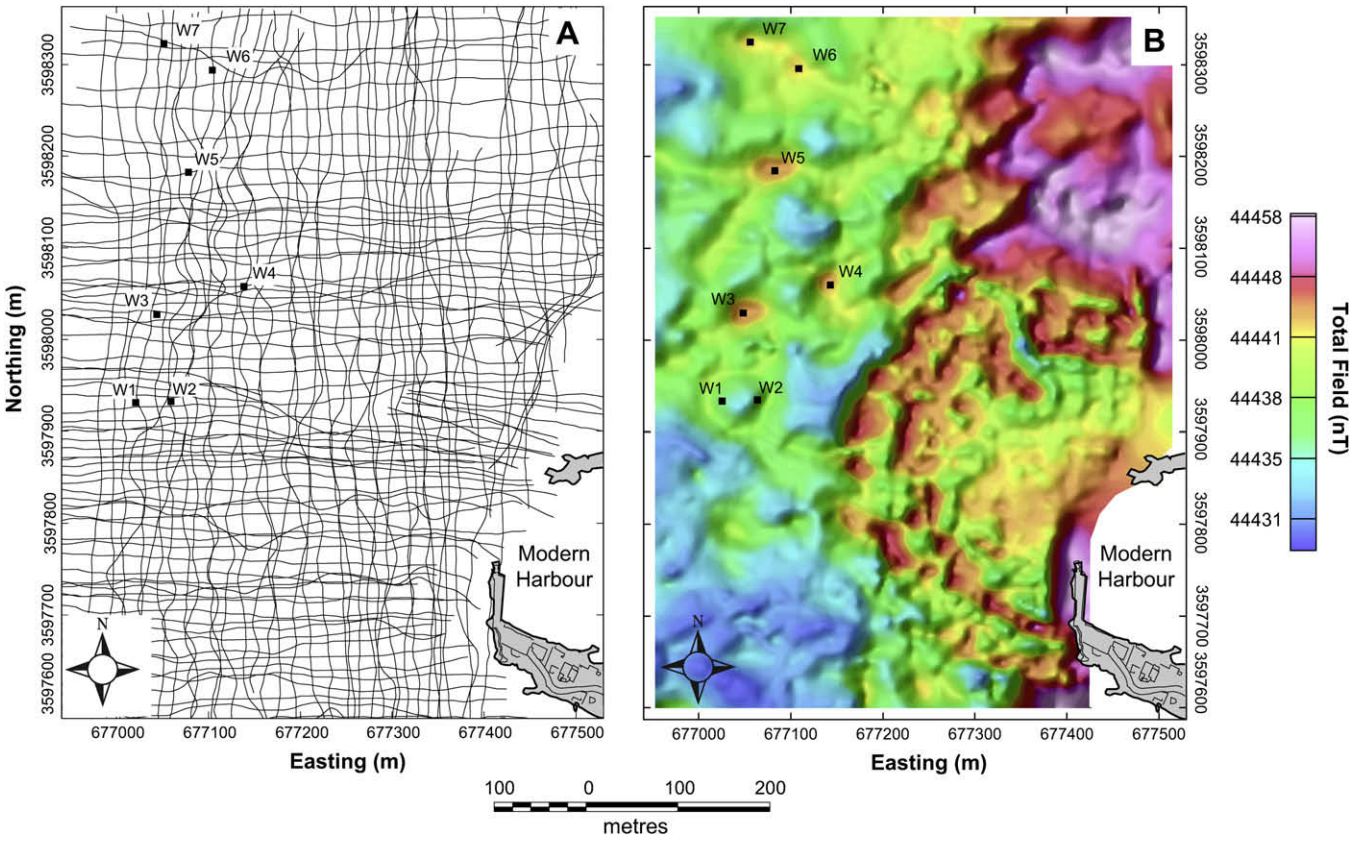

Fig. 2. A. Geophysical survey track lines (nominal line spacing 10–20 m). The along track (inline) interval between magnetic measurements was 0.25–1 m. B. Colour-shaded map showing magnetic total field intensity (nanoteslas, nT) and locations of excavated trenches (W1–W7).

The inshore area to the west has an overall lower magnetic intensity with a number of localized magnetic highs (Fig. 3A). The most conspicuous feature is a roughly circular 'ring-like' magnetic anomaly lying about 100 m to the west of the main Roman harbour mole. The anomaly is about 90 m in diameter and is expressed in the bathymetry map as very low relief, roughly circular mound (Fig. 3B). The magnetic anomaly and the mound are clearly recognizable in the west–east profiles shown in Fig. 4. The seabed relief was enhanced by subtraction of a linear trend surface (i.e. the shoreface slope) from the depth profile (Fig. 4A). This shows that the mound has a maximum relief of ca. 40–60 cm. The corresponding magnetic profile (Fig. 4B) shows a similar 'mounded' appearance, defined by a 6–7 nT increase in magnetic intensity across the mound feature.

Table 1
Results of magnetic susceptibility testing of ballast stone materials, pottery and bottom sediments collected at sites W1–W7. Sample numbers correspond with ballast stones shown in Fig. 7A.

Sample no.	Location	Material	*n*	Mean susceptibility κ (10^{-5} SI)
1	W4	Andesite	8	90.4
2	W3	Limestone	6	0.2
3	W3	Marble	6	1.4
4	W4	Granite	6	267.6
5	W3	Biotite schist	6	467.5
6	W4	Quartzite	6	6.7
7	W4	Limestone	6	0.1
8	W4	Dolostone	6	0.4
9	C92	Med. sand	5	0.1
10	C98	Med. sand	6	0.4
11	RN4	Silt	5	8.7
12	W3	Clay pottery	5	169.6

The intensity of the magnetic anomaly is decreased at its centre and corresponds with a slight bathymetric depression in the mound feature (Fig. 4B).

The ring-like shape of the magnetic anomaly and mounded feature are clearly visible in the perspective 3D images shown in Fig. 5. An overlay of the magnetic intensity on the bathymetry (Fig. 5B) confirms that the magnetic anomaly and the mound are coincident, and that the mound is the source of the magnetic anomaly. Excavation and jet probing in the mound (see below) revealed that the sediment thickness here is greater than 3 m, and that the mound is not the expression of an underlying bedrock protuberance (i.e. bedrock outcrop). The lack of a bedrock prominence below the mound suggests that the magnetic anomaly (Fig. 5B) results from the magnetization of the sediment and ballast materials within the mound itself and not the underlying bedrock. This is supported by the laboratory magnetic testing which shows that ballast rubble within the mound includes a large volume of magnetite-rich rock types (see below).

Several smaller positive magnetic anomalies are present in the area to the northwest of the harbour (sites W3–W7) (Figs. 1A, 3A). These anomalies have an irregular shape in plan and do not have any significant expression in the bathymetry data (Fig. 3B). The magnetic anomalies at locations W3, W4 and W5 (Fig. 3A) are more pronounced than the mounded feature, having a magnetic intensity that is ca. 10–12 nT above the surrounding background levels.

4.2. Stratigraphy

The results of the excavation work are summarized in the stratigraphic profiles in Figs. 6, 7. The stratigraphy at W1 and W2

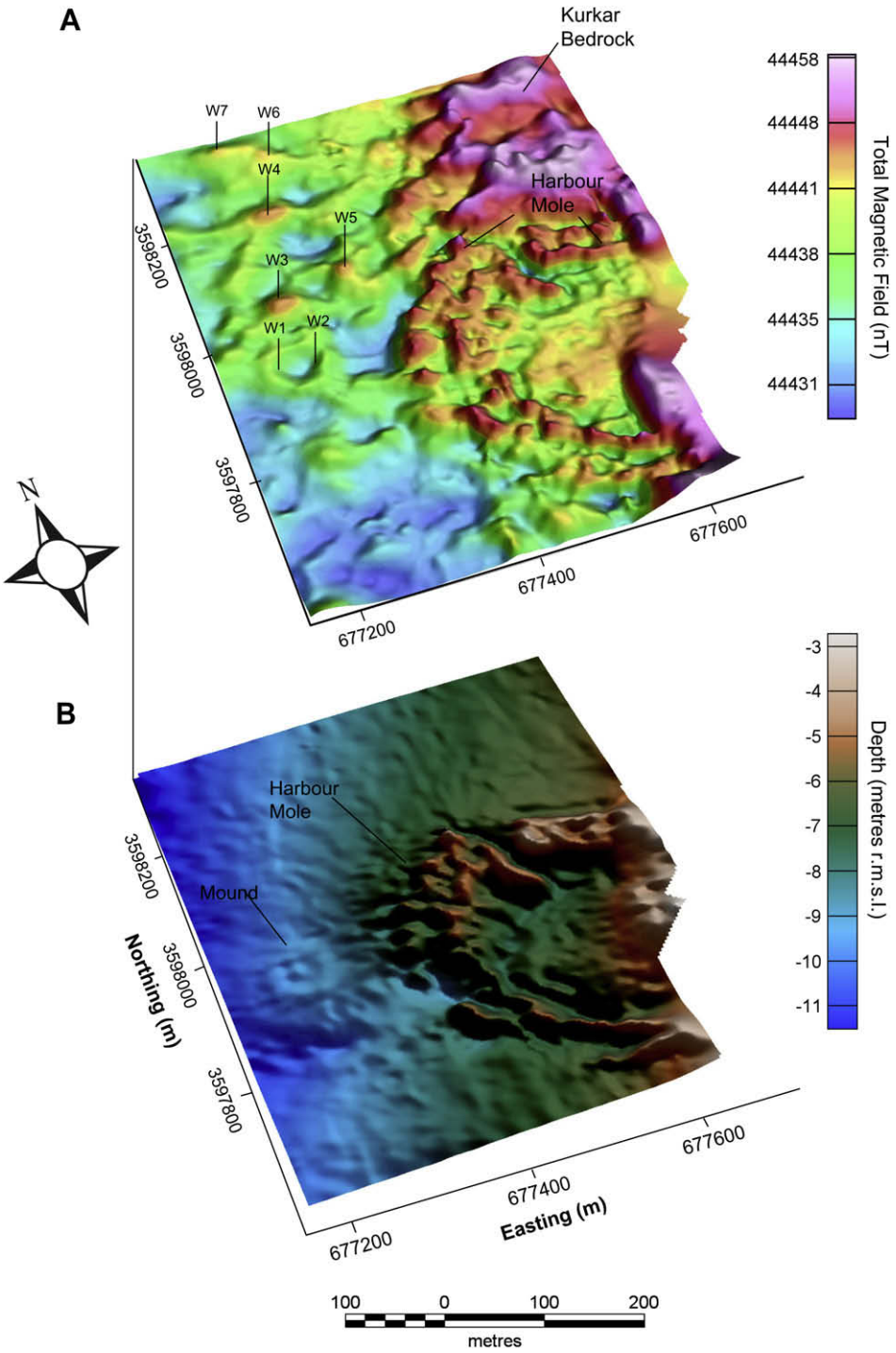

Fig. 3. Colour-shaded surfaces showing: A. Magnetic total field intensity (nT). B. Bathymetry (depth in metres relative to mean sea level). Note low-relief circular mound 100 m to west of submerged harbour mole and corresponding ring-like magnetic anomaly.

consists of an uppermost unit of well-sorted sands (Unit A) overlying a distinctive coarse rubble and pottery layer (Unit B). The rubble layer was 20–60 cm in thickness and contained abundant cobble-sized boulders and pottery fragments. The rubble layer was thickest around the margins of the mound feature but was traceable across the mound as a thin, continuous layer as confirmed by jet probing (Fig. 7). The sand unit below the rubble layer (Unit C) comprises well-sorted sand with silty mud partings and few pottery fragments (Fig. 6). The uppermost sand layer (Unit A) represents the storm active layer that is periodically reworked by storm wave activity on the shoreface (Reinhardt and Raban, 2008).

The boulders within the rubble layer (Unit B; Fig. 6) include a wide range of rock types-local sandstone (kurkar) bedrock, limestone, volcanics (mainly andesite) and large quantities of granitic and metamorphic boulders (gneisses, schist, marble) (Fig. 8A). The granitic and metamorphic boulders are foreign to the Levantine coast and identify the rubble layer as imported ballast

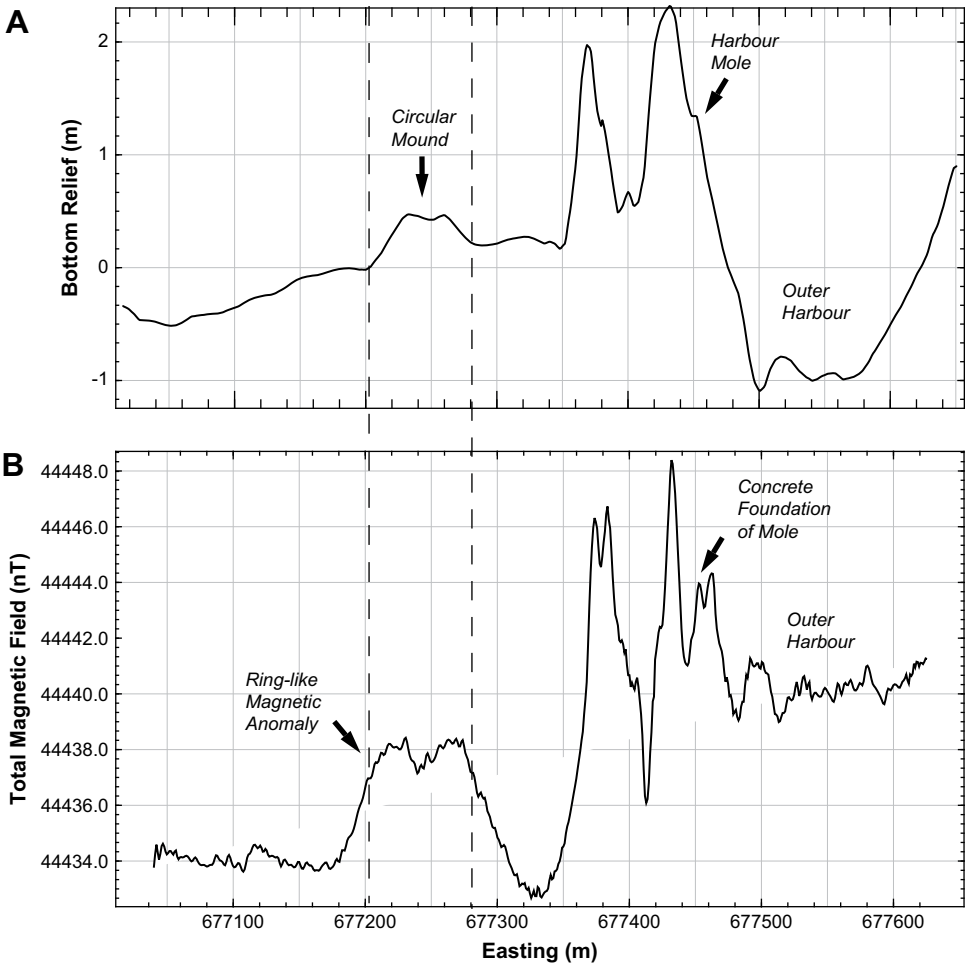

Fig. 4. A. West–east bathymetry profile across ballast mound and southern harbour mole. Bottom relief has been enhanced by subtraction of 1st-order trend surface from depth profile. B. Total field magnetic profile showing increased magnetic intensity over mound due to magnetite-bearing ballast in rubble layer. Much larger magnetic anomalies over harbour moles is due to presence of hydraulic concrete within harbour foundation.

stones jettisoned by merchant ships. It is estimated that about 50% of the ballast rubble layer is made up of these foreign rock types. Most of the boulders are sub-round to well rounded but some angular blocks of quarried sandstone and limestone are also present. Fig. 8A shows a representative collection of some smaller-sized ballast stones retrieved from the Unit B rubble layer. Some large boulders and ashlar blocks (>50 cm diameter) were also present within Unit B but most of the material was of a portable size that could be manually jettisoned over the side of a ship. The mounds are not shipwreck sites as no ship hardware (i.e. nails, sheathing etc.) was found and the ballast was not exposed for any significant period of time on the seabed, as indicated by a lack of bioencrustation and borings on the ballast stones. The lack of bio-encrustation suggests that the ballast materials were deposited then rapidly buried. The ballast stones, which are much coarser than the local bottom sediments (dominantly sand and silt) would have been progressively moved to the base of the storm active layer (Unit A) through winnowing of the sand by storm waves and bottom currents (Reinhardt and Raban, 2008).

The pottery within the ballast rubble layer (Unit B; Fig. 6) consisted of a variety of broken jars and amphoras, and at some localities comprised ca. 20–30% of the deposit volume. The jars included many bag-shaped and elongate Byzantine-age (ca. 330–638 AD) 'Gaza jars' of local origin as well as older Anatolian and Aegean amphorae belonging to the *Late Roman I* and *Late Roman II* types (Talmudic period – ca. 200–330 AD) (Raban, 2004). The Late Roman pottery fragments were concentrated mainly in the lower portion of the rubble layer (Fig. 6) and were much less abundant than the Byzantine pottery fragments in the upper part of the deposit. The crude stratification and age relations of pottery materials within Unit B indicate that is for the most part an *in-situ* deposit that has not been reworked to any great extent. The absence of reworking of the deposit is also supported by the abundance of angular pottery fragments; the rubble layer throughout contained many small angular sherds, some with rounded edges, and also a number of large jar and amphora body fragments as well as some unbroken containers (e.g. bowl; Fig. 8B). The large body fragments lacked wave worn edges and bio-encrustation, indicating limited exposure on the seabed and minimal wave reworking of the deposit. A full interpretation of the pottery materials awaits further work but the available evidence suggests that ballast was accumulated over a relatively long time period, spanning the Late Roman to the Late Byzantine period (ca. 3rd–7th c. AD) (Fig. 6).

Excavations of other magnetic anomalies lying to the north of the mounded feature (sites W3–W7; Fig. 1A) revealed a similar stratigraphy, comprising well-sorted sands (Units A and C) with an intervening 20–70 cm thick ballast rubble layer (Unit B; Figs. 6, 7). The rubble layer composition at these sites was similar to W1 and W2, comprising more than 50% igneous and metamorphic boulders

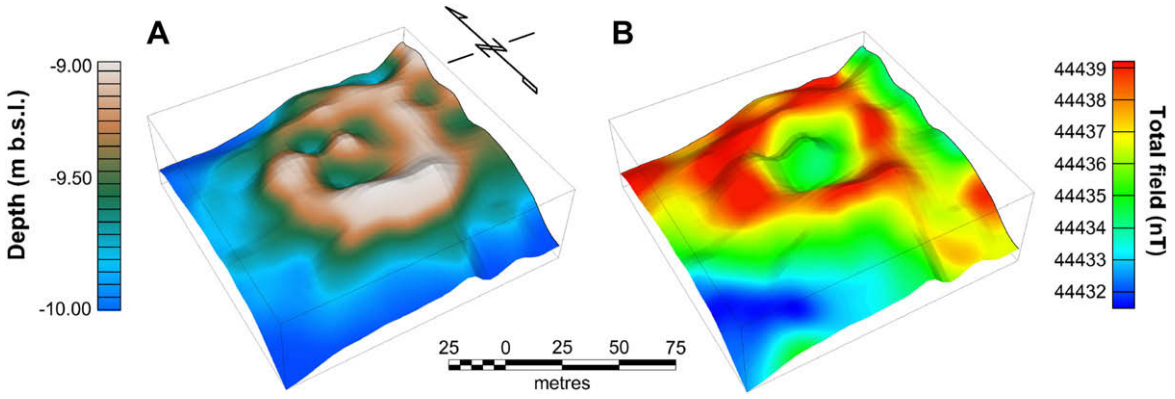

Fig. 5. A. Perspective view of ballast mound bathymetry (north to top of page). Relief across mound is about 0.5–1 m. B. Magnetic total field map overlaid on top of bathymetry, showing 'ring-like' magnetic anomaly (ca. 6–7 nT) produced by igneous and metamorphic boulders within ballast rubble layer.

and about 50% sedimentary rock types. The rubble layer was notably thicker at sites W4 and W7 and was encountered at a shallower depth than site W2 (Fig. 6). The pottery in the Unit B rubble layer at these locations was very similar to that of W2 and included large angular fragments of Late Roman jars and amphoras and abundant Byzantine-age 'Gaza' type containers (e.g. Fig. 8B) (Raban, 2004).

Excavations and jet probing at W4, W6 and W7 revealed the presence of two further stratigraphic units (Units D and E; Fig. 6) not present at sites W1 and W2. Unit D consisted of a thick (40–60 cm) shell layer containing abundant *Glycymeris* sp. bivalve shells. The shell layer contained a few pottery fragments, including sherds of 'Eastern Sigillata B' and Early Roman bag-shaped jars of 'Riley 1A' type that are characteristic of the 1st and early 2nd c. AD (Raban, 2004). The shell layer has distinctive taphonomic characteristics, including an abundance of whole articulated and disarticulated *Glycymeris* sp. shells and many angular shell fragments showing evidence of stress fracturing (Reinhardt et al., 2006). Reinhardt et al. (2006) have interpreted these taphonomic characteristics as evidence for catastrophic scour of the shoreface and

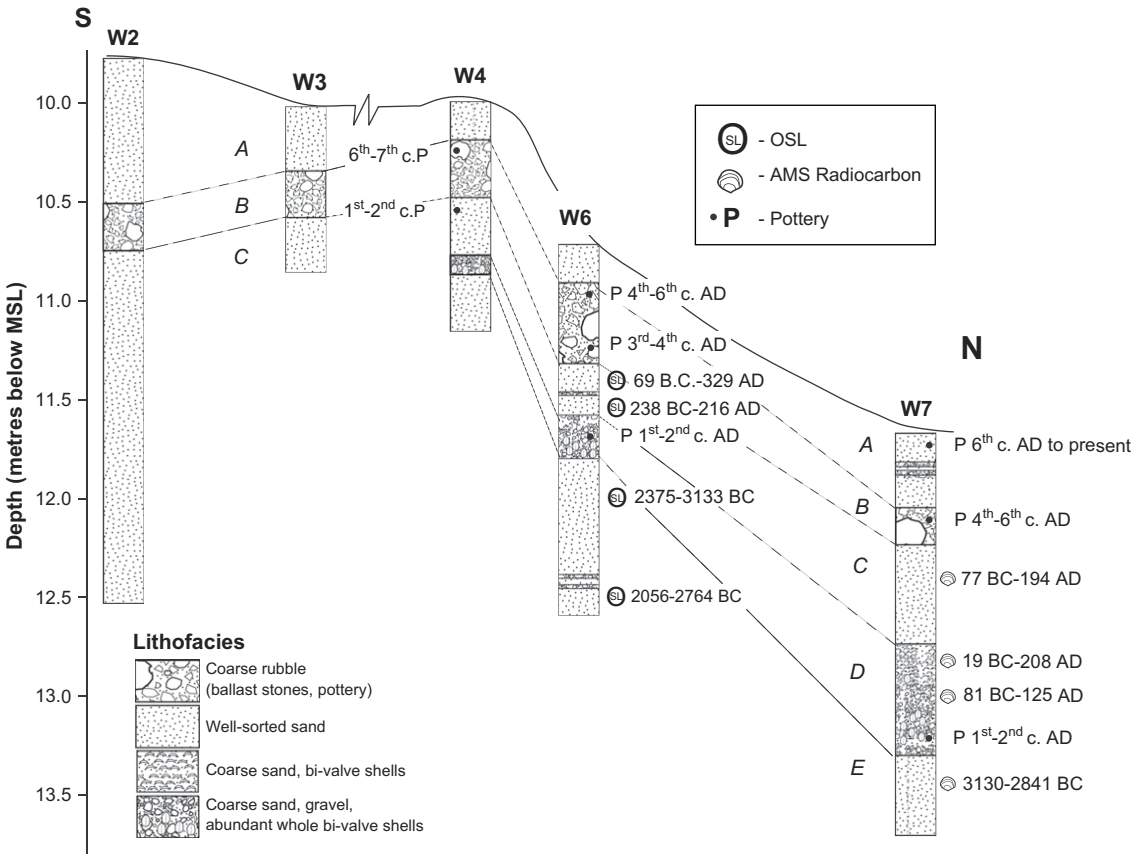

Fig. 6. South–north profile showing stratigraphy of excavated trenches (locations in Fig. 1A). Ballast rubble layer (Unit B) consists of a variety of ballast stone types and abundant pottery fragments. Pottery evidence and absolute dates (AMS ^{14}C and OSL) constrain the age of the ballast deposit to the 2nd–7th c. AD.

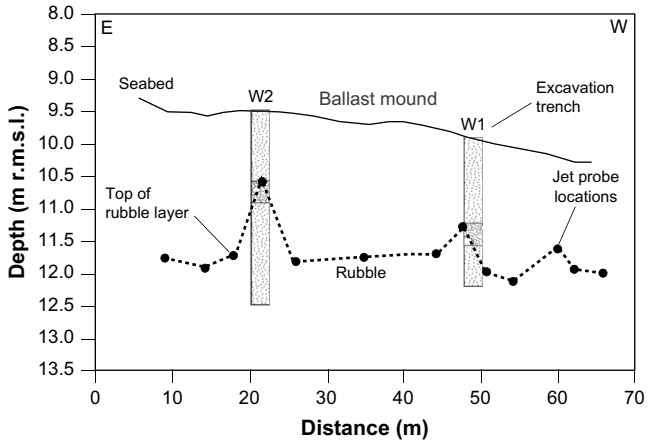

Fig. 7. Jet-probe profile (east to west) across large ballast mound at W1–W2 (location in Fig. 1A). Dashed line shows depth to top of ballast rubble layer.

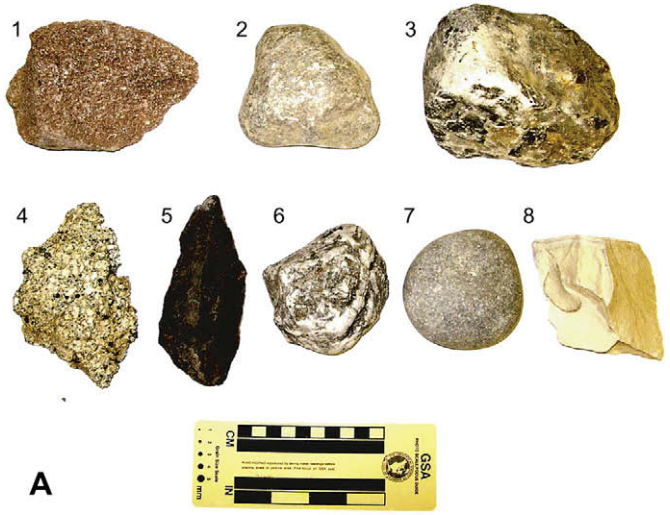

Fig. 8. A. Collection of small ballast stones from locations W3 and W4, showing range of lithologic materials. Lithologies and magnetic susceptibility values are given in Table 1. Ballast material sizes range from pebbles to boulders up to 0.5 m diameter. B. Byzantine amphora and jar fragments and bowl recovered from ballast rubble layer at location W7.

rapid deposition by a tsunami event that partially destroyed Caesarea's harbour in the 2nd c. AD. The tsunami was likely triggered by a large magnitude earthquake in Syria, which destroyed the city of Antioch in 115 AD (Ambraseys and Jackson, 1998). The tsunami shell layer rests erosively across a unit of well-sorted sand (Unit E; Fig. 6) that is completely devoid of pottery or other cultural materials. AMS ^{14}C dates obtained on shell materials from the lowermost Unit E sand indicate it is a much older deposit, dating to the 3rd to 4th millennium BC. The large difference in ages between the overlying shell-rich tsunamite (Unit D) and this unit indicates a significant erosional hiatus and extensive scour of the shoreface by the 2nd c. tsunami event.

4.3. Chronology

The age of the ballast rubble layer (Unit B; Fig. 6) was constrained using pottery evidence and ^{14}C and OSL dates obtained on underlying deposits (Raban, 2004; Reinhardt et al., 2006; Rink and Reinhardt, 2008). AMS ^{14}C dating of bivalve shells at site W7 indicates that the sand unit (Unit C) directly below the ballast rubble layer was deposited sometime during the late 1st c. BC–2nd c. AD (Fig. 6). OSL dates on Unit C sands at site W6 yielded a broader range of ages (69 BC–329 AD), which in part reflects the larger systematic errors with this method. The oldest pottery fragments found within the basal portion of the Unit B were of 3rd–4th c. AD in age (e.g. W6; Fig. 6). When combined with the absolute ages, the pottery evidence suggests an onset of ballast accumulation and deposition of Unit B in the Late Roman period (ca. 200–330 AD). The abundance of 4th–6th c. AD pottery within the upper portion of Unit B also seems to point to a significant increase in ballast deposition during the Byzantine Period. The onset of ballast accumulation coincided with a decline in the state of the Caesarea's harbour following the 115 AD tsunami event (Reinhardt et al., 2006) and a shift to a more intensive use of the area outside the harbour as an anchorage during a later peak in trading activity in the 4th c. AD (see Discussion).

4.4. Magnetic properties

The results of magnetic susceptibility testing of ballast stones and sediment samples are summarized in Table 1. The natural shoreface sediments (Units A and C) comprising well-sorted quartz sand and silt had uniform low-magnetic susceptibilities ranging from 0.1 to 8.7 $\times 10^{-5}$ (SI). The ballast stones collected from within the ballast rubble layer (Unit B), in contrast, showed a much wider range of susceptibility values (0.1 to 467.5 $\times 10^{-5}$ SI) reflecting the different ballast lithologic compositions (Fig. 8A). The highest susceptibility values as expected, were obtained on crystalline igneous and metamorphic boulders ($>200 \times 10^{-5}$ SI), which are rich in magnetite and illmenite. The volcanic rock samples were also characterized by moderate susceptibilities ($>90 \times 10^{-5}$ SI), as were the clay pottery sherds (169.6 $\times 10^{-5}$ SI) (Table 1).

Ballast stones consisting of sedimentary rock types (sandstone, limestone) yielded much lower susceptibilities ($<2 \times 10^{-5}$ SI) comparable to values for the natural bottom sediments at Caesarea. These materials are too low in magnetic susceptibility to account for the elevated magnetic intensity measured over the ballast accumulations (Fig. 3A). The igneous and metamorphic boulders within the ballast layer (Unit B; Fig. 6) have a much larger magnetic contrast with the natural background sediments (Table 1) and are the most likely source of the observed anomaly patterns (Fig. 3A). Clay pottery materials of intermediate magnetic susceptibility (Table 1) likely also contribute significantly to the magnetic anomalies, as they make up a significant part of the total volume of the ballast layer. The magnetic susceptibilities of the underlying

strata (Units D and E; Fig. 6) are considered to be negligible, as they consist chiefly of low susceptibility sands and carbonate shell materials.

We interpret the increase in magnetic intensity across the ballast mounds (ca. 2–12 nT) to result from the induced magnetization of a large volume of magnetite-bearing igneous and metamorphic ballast stones and pottery within the ballast layer. The remanent magnetizations of volcanic boulders (i.e. andesites) and clay pottery fragments may also contribute to the total field anomaly (e.g. Bevan, 1994; Hesse et al., 1997) but cannot be determined from the magnetic susceptibility testing, which measures only induced magnetization. Due to the essentially random orientations of volcanic boulders and pottery materials within the ballast layer, the thermoremanent component of magnetization is likely to be very weak in comparison to the induced magnetization produced by the large contrast in magnetic susceptibility.

5. Discussion

The magnetic survey and underwater excavation work at Caesarea have revealed that a large area of the shelf seaward of the Roman harbour is underlain by thick ballast accumulations (Figs. 3A, 6). The age constraints provided by pottery and ^{14}C and OSL dates indicate deposition of the ballast over a span of several centuries, beginning sometime in the 3rd–4th c. AD (Late Roman Period) and extending well into the Late Byzantine period. The total volume of the ballast rubble layer is substantial and is estimated at more than 1.6×10^6 m^3 based on the extent and average thickness of Unit B (ca. 40 cm) (Fig. 6). As discussed in the following sections, these results have important archaeological implications for understanding the operation of Caesarea's harbour in antiquity and how it's decline and poor state of repair in the early 2nd c. AD may have affected subsequent shipping activities.

5.1. Anchorage areas at Caesarea

The wide extent and thickness of the ballast layer at Caesarea (Fig. 3A) indicates that the area outside of the harbour was in regular use by the 3rd c. AD as a mooring site for merchant ships. The presence of discrete ballast mounds also suggests that jettisoning of ballast may have been restricted to certain designated 'lightening areas'. These anchorage areas were likely regulated by the harbour authority to discourage the dumping of ballast inside the harbour and to avoid the need for expensive dredging of the harbour bottom. It is known from archaeological reconstructions that the Herodian harbour included an engineered sluicing system that diverted currents into the harbour basin to reduce siltation (Raban, 1999). Given that natural siltation was a problem in the harbour, it would also seem logical that ballast dumping would be restricted to outside the harbour, as bouldery ballast materials would rapidly accelerate the accumulation of fine sediments in the main basin. Such a policy may have been necessary given the important role that Caesarea played as a busy trans-shipment port for goods sailing between Judea and Rome (Raban, 1999).

The thickness and wide extent of the ballast deposit is consistent with Caesarea's importance as an export port dealing in goods bound for Rome (Raban, 1999). Based on artifactual evidence Oleson (1996) identified two main peaks in trading activity at Caesarea; one in the 1st c. BC–1st c. AD, and a later peak in the 4th–5th c. AD. The available pottery and dating evidence suggest that at least some of the ballast in the lower portion of Unit B (Fig. 6) is likely from the earlier period of trading activity, following the construction of the harbour. The relative dearth of pottery fragments from this early phase may indicate that on loading and offloading of goods was carried out while the ships were docked within the main harbour basin.

The abundance of Byzantine pottery in the upper part of Unit B can be correlated with the later trade peak in the 4th–5th c. AD (Fig. 6). The substantial accumulation of pottery-laden ballast

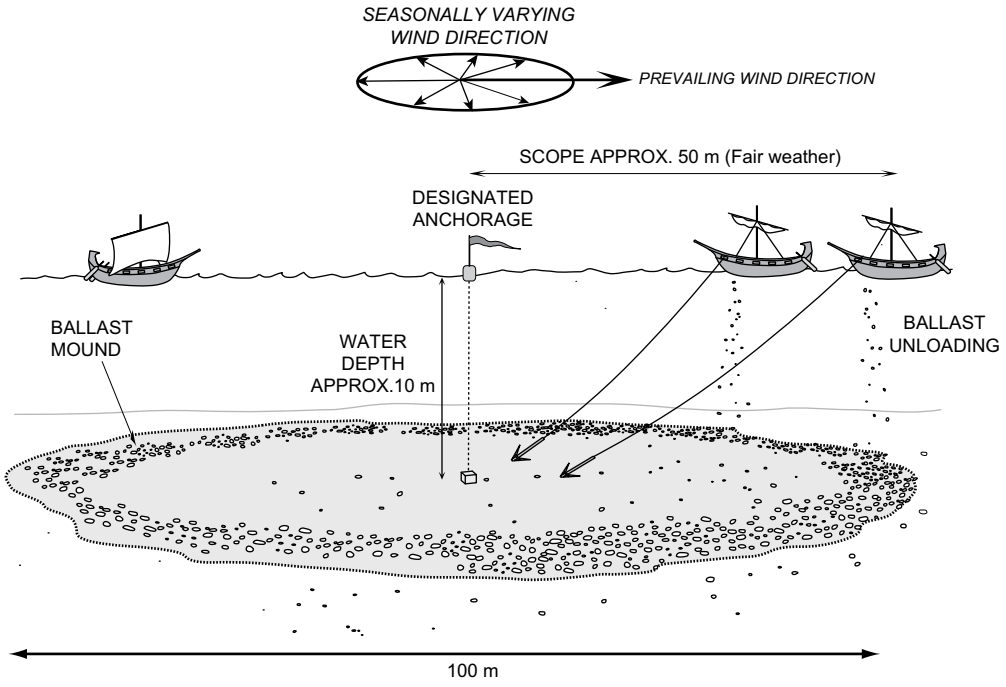

Fig. 9. Conceptual model for deposition of ballast mound outside Caesarea's harbour. Ships anchored around a designated mooring site drift in a range of directions, depending on the prevailing wind and current conditions on coast. A ring-like ballast accumulation is formed over time as ballast is unloaded by ships anchored at different positions around the mooring. The mound diameter is a function of the water depth and anchor scope (ca. 1:5 ratio in fair weather conditions).

indicates that ships were moored outside the harbour during this period, and that the harbour basin no longer provided a safe anchorage. It has been documented based on several lines of evidence that Caesarea's harbour was partially destroyed in the early 2nd c. AD, as a result of earthquake damage and a large tsunami that impacted the Judean coastline in 115 AD (Raban, 1991; Mart and Perecman, 1996; Reinhardt and Raban, 1999; Reinhardt et al., 2006). The tsunami was recorded in the Talmud and caused widespread erosion of the shoreline at Caesarea that undermined and damaged the harbour's protective breakwater structures (Reinhardt et al., 2006). Other historical sources also point to the poor state of repair of the harbour following this event. In the early 6th c. AD Procopius of Gaza, an early Christian orator, reported that the harbour was in disrepair, and that he watched ships wreck regularly on the harbour moles (Holum et al., 1988; Hohlfelder, 1988). Ships were no doubt wary of the harbour, with its ruined breakwater only shallowly submerged below the waves, a hazard which could rip the bottom out of a merchantman. It is likely that ships anchored outside of the harbour during this period, as it represented a navigational hazard, particularly for the larger, less maneuverable merchant vessels. Compelling evidence supporting this was the discovery of a Roman merchantman wreck on top of the main harbour mole (Raban, 1999) (Fig. 1A). The wreck site, dated to ca. 100 AD based on a cargo of lead ingots, indicates that the harbour mole was at least partly submerged by that time and was no longer functioning as a protective breakwater. A number of other shipwrecks dating from the 3rd c. AD have also been discovered on the harbour moles (Raban, 1989) showing that the harbour was a serious navigational hazard by this time.

According to Procopius, the Byzantine Emperor Anastasius I (AD 491–518) seeing the poor state of Caesarea's port provided the means for the renovation of the harbour. Based on archaeological evidence this included both reconstruction of the northern mole and part of the inner harbour basin (Reinhardt and Raban, 1999). The shallow inner harbour 'lagoon' (Fig. 1A) would have provided a sheltered environment where lighters could on- and off-load the larger merchantmen riding at anchor outside of the harbour. It is also likely that during this period ships still used the renovated harbour basin as an anchorage, but it would have been restricted to smaller, more maneuverable vessels that required less draft.

5.2. Origin of ballast mound

The origin of the circular ballast accumulation (Fig. 5) is not fully understood, but its size and age (Late Roman–Late Byzantine) indicate a sustained use of the area outside the harbour as an anchorage area. The presence of a buried architectural feature (e.g. circular tower base) was initially suspected but was ruled out by excavations and jet probing (Fig. 7), which found no evidence for buried wall features. One possible explanation for the roughly circular form of the mound is that the feature may represent a designated mooring site where ships were required to off-load ballast prior to lading as shown in the conceptual drawing in Fig. 9. Because of daily and seasonal variations in the wind directions on the coast at Caesarea, ships anchored around a fixed mooring would occupy different areas of the anchorage at different times. A circular ballast mound could thus be accumulated as ships discharged ballast at different times and under different prevailing wind directions. The size (diameter) of the mound would reflect some average radius as determined by the scope required to anchor (Fig. 9). Given an estimated water depth of 7–10 m (Fig. 1A), the anchor scope length under fair weather conditions would have been approximately 35–50 m using a 5:1 ratio. It is noted that this length is comparable to the approximate radius of the mound feature (ca. 45 m) (Fig. 5).

6. Summary

The primary contribution of this paper has been to demonstrate that ancient ship ballast deposits can be detected and mapped on the seabed using magnetic survey methods. Magnetic surveys at Caesarea have identified several magnetic anomalies in the area seaward of the main harbour that mark the location of ballast deposits and ship anchorage areas (Fig. 1A). The available sediment dates and pottery evidence suggest that the onset of ballast deposition was in the late 2nd–3rd c. AD, following the partial destruction of Caesarea's harbour and a decline in its use as a safe anchorage area. The main phase of ballast accumulation occurred in the 4th–5th c. AD, coinciding with a renewed economic activity of the harbour. Due to decline in the state of the harbour after the 2nd century merchant vessels arriving at the port would have been forced to ride at anchor outside the harbour while goods were transferred to the port via small lighters. The accumulation of ballast in discrete mounds indicates that ballast dumping may have been regulated and restricted to designated 'lightening areas'.

Acknowledgments

This work was supported through Natural Science and Engineering Research Council of Canada (NSERC) research grants to JIB and EGR and an anonymous donor. The authors thank students S. Collins, P. van Hengstum, A. Kingston for field and laboratory assistance and the staff of the Recanati Institute (S. Breitstein, A. Yurman) and Marine Magnetics Ltd. (D. Hrvoic, M. Marlowe) for technical support with marine survey operations. Processing of geophysical data was made possible through academic software grants from Geosoft Canada Ltd.

References

Avnimelech, M.A., 1962. The main trends in the Pleistocene-Holocene history of the Israeli coastal plain. Quaternaria 6, 479.
Ambraseys, N.N., Jackson, J.A., 1998. Faulting associated with historical and recent earthquakes in the Eastern Mediterranean region. Geophys. J. Int. 133, 390–406.
Ballard, R.D., McCann, A.M., Yoerger, D., Whitcomb, L., Mindell, D., Oleson, J., Singh, H., Foley, B., Adams, J., Peichota, D., Giangrande, C., 2000. The discovery of ancient history in the deep sea using advanced deep submergence technology. Deep-Sea Res. 47, 1591–1620.
Bertrame, C., Gaddi, D., 2002. Report on the research campaign on the Napoleonic brick, Mercure, wrecked off Lignano, Udine, Italy in 1812. Int. J. Naut. Arch. 31, 61–73.
Bevan, B., 1994. The magnetic anomaly of brick foundation. Arch. Prosp. 1, 93–104.
Boyce, J.I., Reinhardt, E.G., Raban, A., Pozza, M.R., 2004. Marine magnetic survey of a submerged Roman harbour, Caesarea Maritima, Israel. Int. J. Naut. Arch. 33, 122–136.
Brandon, C., 1999. Pozzolana, lime, and single-mission barges (area K). In: Holum, K., Raban, A., Patrich, J. (Eds.), Caesarea Papers, vol. 2. J. Roman Arch., Supplementary Series 35, pp. 169–78.
Breiner, S., 1973. Applications Manual for Portable Magnetometers. Geometrics Ltd., Sunnyvale, California, 58 pp.
Callahan, J.E., Miller, J.W., Craig, J.R., 2001. Ballast stone studies from North Carolina shipwreck 0003 BUI, the Queen Anne's Revenge: hand specimen, x-ray, petrographic, chemical, paramagnetic and ^{40}K–^{40}Ar age results. Southeastern Geol. 40, 49–58.
Conaghan, P.J., Delaney, W., Hawlader, H.M., 1998. Geoarchaeological confirmation of shipwreck identity, Cockburn Reef, far-north Queensland, Australia. Geoarchaeology 13, 161–199.
Cordell, L.E., 1985. Techniques, applications, and problems of analytical continuation of New Mexico aeromagnetic data between arbitrary surfaces of very high relief. In: Proceedings of the International Meeting on Potential Fields in Rugged Topography. Institute of Geophysics, University of Lausanne, Switzerland, pp. 96–99. Bulletin no. 7.
Emery, K.O., Kaye, C.A., Loring, D.H., Nota, D.J.G., 1968. European Cretaceous flints on the coast of North America. Science 160, 1225–1228.
Grauch, V.J.S., Campbell, D.L., 1984. Does draping aeromagnetic data reduce terrain-induced effects? Geophysics 49, 75–80.
Gvirtzman, G., Shachnai, E., Bakler, N., Ilani, S., 1983. Stratigraphy of the kurkar group (quaternary) of the coastal plain of Israel. Geol. Surv. Israel Curr. Res., 70–82. 1983–84.

Hesse, A., Barba, L., Ortiz, L., Link, K., 1997. A magnetic and electrical study of archaeological structures at Loma Alta, Michoacan. Mexico Arch. Prosp. 4, 53–67.
Hohlfelder, R.L., 1988. Procopius, De Aedificiis, 1.11.18–20: Caesarea Maritima and the building of harbours in late antiquity. Mediterranean Hist. Rev. 3, 54–62.
Hohlfelder, R.L., 1999. Building sebastos: the cyprus connection. Int. J. Naut. Arch. 28, 154–163.
Holum, K.G., Hohlfelder, R.L., Bull, R.J., Raban, A., 1988. King Herod's Dream: Caesarea on the Sea. W.W. Norton, New York, 244 pp.
Keith, D.H., Simmons, J.J., 1985. Analysis of hull remains, ballast and artifact distribution of a 16th-century shipwreck, Molasses Reef, British West Indies. J. Field Arch. 12, 411–424.
Kingsley, S.A., 2003. The Dor D shipwreck and Holy Land wine trade. Int. J. Naut. Arch. 32, 85–90.
Lamb, W.R., 1986. Oft-spurned ballast is seen as another data source. INA Newsletter 13, 12–13.
Lamb, W.R., Keith, D.H., Judy, S.A., 1990. Analysis of the ballast of the Molasses Reef wreck. Natl. Geogr. Res. 6, 291–305.
Lazareth, C.E., Mercier, J.C., Garnaud, S., 2001. A geochemical study of larkivite from Brouage (France): evidence for European commercial sea links in Early Modern times. Earth Planet. Sci. 332, 733–738.
Luyendyk, A.P.J., 1997. Processing of airborne magnetic data. AGSO J. Australian Geol. Geophys. 17, 31–38.
Mart, Y., Perecman, I., 1996. Neotectonic activity in Caesarea, the Mediterranean coast of central Israel. Tectonophysics 254, 139–153.
McManus, J., 1999. Coarse estuary mouth ballast gravel deposits: a sourcing case history. Estuar. Coast. Shelf Sci. 48, 677–682.
Oleson, J.P., 1996. Artifactual evidence for the history of the harbors of Caesarea. In: Raban, A., Holum, K.G. (Eds.), Caesarea Maritima; a Retrospective After Two Millennia. E.J. Brill, Leiden, pp. 359–377.
Parker, A.J., 1981. Stratification and contamination in ancient Mediterranean shipwrecks. Int. J. Naut. Arch. 10, 309–335.
Pilkington, M., Thurston, J.B., 2001. Draping corrections for aeromagnetic data: line- versus grid-based approaches. Exp. Geophys. 32, 95–101.
Pozza, M.R., Boyce, J.I., Morris, W.A., 2004. Lake-based magnetic mapping of contaminated sediment distribution, Hamilton Harbour, Ontario, Canada. J. Appl. Geophys. 57, 23–41.
Raban, A., 1989. The Harbours of Caesarea Maritima, Results of the Caesarea Ancient Harbor Excavation Project 1980–85, the Site and the Excavations, vol. 1. British Archaeological Reports, Oxford, No. 491, International Series, 517 pp.
Raban, A., 1991. The subsidence of Sebastos. Thracia Pontica 4, 339–366.
Raban, A., 1992. Sebastos, the royal harbour at Caesarea Maritima – a short-lived giant. Int. J. Naut. Arch. 21, 111–124.
Raban, A., 1994. Sebastos, the Herodian harbour of Caesarea: construction and operation. Sefunim 8, 45–59.
Raban, A., 1999. Lead ingots from wreck site (K8). In: Holum, K.G., Raban, A., Patrich, J. (Eds.), Caesarea Papers, vol. 2. J. Roman Arch., Supplementary Series 35, pp. 179–188.
Raban, A., 2004. The underwater excavations at Caesarea Maritima, 2003. RIMS Newsletter 30, 14–17. Haifa University.
Raban, A., Reinhardt, E.G., McGrath, M., Hodge, N., 1999. The underwater excavations, 1993–94. In: Holum, K.G., Raban, A., Patrich, J. (Eds.), Caesarea Papers, vol. 2. J. Roman Arch., Supplementary Series 35, pp. 52–168.
Raveh, K., Kingsley, S.A., 1991. The status of Dor in late antiquity: a maritime perspective. Biblical Arch. 54, 198–207.
Raveh, K., Kingsley, S.A., 1992. The wreck complex at the entrance to Dor harbour, Israel: preliminary results. Int. J. Naut. Arch. 21, 309–315.
Reinhardt, E.G., 1999. Stratigraphic excavation of the outer harbor deposits: preliminary report (1994). In: Holum, K.G., Raban, A., Patrich, J. (Eds.), Caesarea Papers, vol. 2. J. Roman Arch., Supplementary Series 35, pp. 189–197.
Reinhardt, E.G., Raban, A., 1999. Destruction of Herod the Great's harbour at Caesarea Maritima, Israel – geoarchaeological evidence. Geology 27, 811–814.
Reinhardt, E.G., Raban, A., 2008. Site formation and stratigraphic development of Caesarea's ancient habor. In: Holum, K.G, Stabler, J.A, Reinhardt, E.G. (Eds.) Caesarea Reports and Studies, British Archeological Reports, 1784, pp. 155–182.
Reinhardt, E.G., Goodman, B.N., Boyce, J.I., Lopez, G., van Hengstum, P.J., Rink, W.J., Mart, Y., Raban, A., 2006. The tsunami of 13th December A.D. 115 and the destruction of Herod the Great's harbor at Caesarea Maritima, Israel. Geology 34, 1061–1064.
Rink, W.J., Reinhardt, E.G., 2008. Optical luminescence dating of sediments from Herod's Harbor. In: Holum, K.G, Stabler, J.A, Reinhardt, E.G. (Eds.) Caesarea Reports and Studies, Brtitish Archeological Reports, 1784, pp. 183–188.
Royal, J.G., 2006. The remote-sensing survey of the south-eastern Bozburun Peninsula, Turkey: shipwreck discoveries and their analyses. Int. J. Naut. Arch. 35, 195–217.
Sonnenburg, E.P., Boyce, J.I., 2008. Data-fused digital bathymetry and side-scan sonar as a base for archaeological inventory of submerged landscapes in the Rideau Canal, Ontario, Canada. Geoarchaeology 23, 654–674.
Stanley, J.D., Bernasconi, M.P., 2004. Holocene depositional patterns and evolution in Alexandria's eastern harbor, Egypt. J. Coastal Res. 22, 283–297.
Telford, W.M., Geldart, L.P., Sheriff, R.E., 1998. Applied Geophysics. Cambridge University Press, 770 pp.
Ugalde, H., Morris, W.A., 2008. An assessment of topographic effects on airborne and ground magnetic data. The Leading Edge 27, 76–79.
Votruba, G.F., 2007. Imported building materials of Sebastos harbour, Israel. Int. J. Naut. Arch. 36, 325–335.